

# Decoupling Continual Semantic Segmentation

Yifu Guo<sup>1,2,\*</sup>, Yuquan Lu<sup>1,2,\*</sup>, Wentao Zhang<sup>1</sup>, Zishan Xu<sup>2</sup>, Dexia Chen<sup>1</sup>, Siyu Zhang<sup>3</sup>, Yizhe Zhang<sup>4</sup>, Ruixuan Wang<sup>1,†</sup>

<sup>1</sup>Sun Yat-sen University, <sup>2</sup>Shanghai Jiao Tong University,

<sup>3</sup>Southwest University, <sup>4</sup>University of Notre Dame

{20223801024}@m.scnu.edu.cn, {wangruix5}@mail.sysu.edu.cn <sup>\*</sup>

## Abstract

Continual Semantic Segmentation (CSS) requires learning new classes without forgetting previously acquired knowledge, addressing the fundamental challenge of catastrophic forgetting in dense prediction tasks. However, existing CSS methods typically employ single-stage encoder-decoder architectures where segmentation masks and class labels are tightly coupled, leading to interference between old and new class learning and suboptimal retention-plasticity balance. We introduce **DecoupleCSS**, a novel two-stage framework for CSS. By decoupling class-aware detection from class-agnostic segmentation, DecoupleCSS enables more effective continual learning, preserving past knowledge while learning new classes. The first stage leverages pre-trained text and image encoders, adapted using LoRA, to encode class-specific information and generate location-aware prompts. In the second stage, the Segment Anything Model (SAM) is employed to produce precise segmentation masks, ensuring that segmentation knowledge is shared across both new and previous classes. This approach improves the balance between retention and adaptability in CSS, achieving state-of-the-art performance across a variety of challenging tasks. Our code is publicly available at: <https://github.com/euyis1019/Decoupling-Continual-Semantic-Segmentation>.

## 1. Introduction

Continual Semantic Segmentation (CSS) addresses a practical scenario where new segmentation tasks with novel classes emerge over time [5, 13, 63]. A machine learning model must effectively learn these new classes while retaining previously learned old knowledge, ensuring that old knowledge is not forgotten. CSS has many real-world applications, such as autonomous driving [3], medical imag-

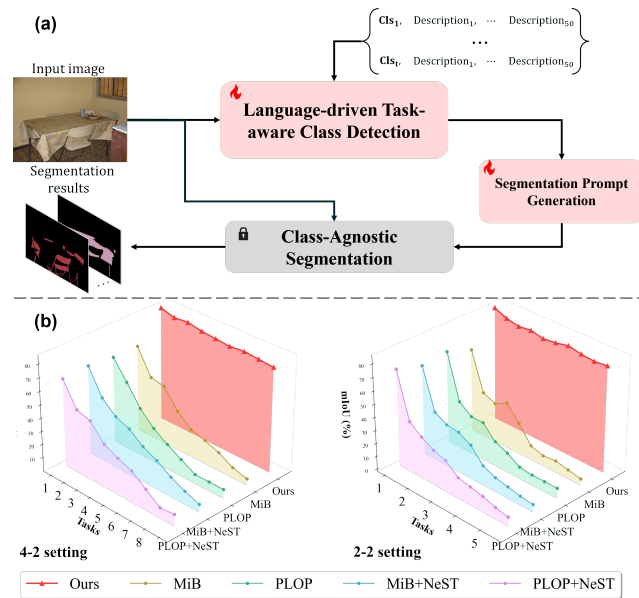


Figure 1. **Overview of the proposed method.** (a) The overall architecture. (b) Representative results on challenging settings (2-2 and 4-2) for CSS on Pascal VOC 2012.

ing [16, 47] and remote sensing [45]. As a dense prediction task, CSS is particularly susceptible to semantic shifts, where the model's understanding of class relationships may evolve over time. Furthermore, similar to other continual learning tasks, CSS faces the challenge of catastrophic forgetting, where previously learned knowledge can be influenced and overwritten by new information.

Several methods have been proposed to address the challenges in CSS. Data replay [30, 71] is effective but requires storing raw data/features, leading to linear memory growth and potential privacy concerns. Regularization techniques [4] penalize deviations in important model parameters for old classes, but often struggle to balance retention

<sup>\*</sup>Equal contribution.

<sup>†</sup>Corresponding author.

and plasticity. Pseudo-labeling [13, 44] and knowledge distillation [43, 48, 54] preserve old class knowledge by generating pseudo-labels or distilling knowledge from the old model, but still can cause background class drift when uncertain pixels are labeled as background. To mitigate this, the background weight transfer method [34, 60] initializes new class classifiers with background weights. However, it may mix new class features with background features, especially in cases of limited training data.

Most prior CSS methods employ a single-stage (encoder-decoder) segmentation paradigm, as seen in models such as DeepLab-V3 [9]. In these methods based on pixel-level multi-class classification, segmentation masks (intra-class consistency) and class labels (inter-class discrimination) are tightly coupled within a shared set of model parameters. This creates a significant challenge in the continual learning setting where the supervisory signals needed for inter-class discrimination between old and new categories are systematically removed, which partly causes catastrophic forgetting.

To tackle the CSS challenge, we propose a two-stage segmentation framework called DecoupleCSS in which class-aware perception (Figure 1a, red components as the first stage) is decoupled from Class-Agnostic Segmentation (CAS, gray component in Figure 1a as the second stage), enabling a separation of concerns where continual learning targets the class-aware detection phase, while the segmentation module can be shared across old and new tasks. In the first stage, class-specific semantic textual information is used to guide an adapted image encoder to extract class-relevant features. Note that different tasks share the same pre-trained frozen image encoder but have their own task-specific visual adapters which are optimized during continual learning. Such class-relevant visual features are then used to detect existence of classes in the input image and to generate class-aware and location-specific prompts. In the second stage, these prompts activate SAM to generates precise segmentation masks. Our contributions are summarized below.

- At the framework level, this study presents a novel perspective and approach for Continual Semantic Segmentation (CSS). We advocate using class-agnostic foundation models (e.g., SAM) as a cornerstone for practical CSS research and propose a separation of class-aware and class-agnostic components in CSS learning. This explicit decoupling enables effective, focused continual learning for detection (class-aware), while segmentation knowledge (class-agnostic) is shared across classes.
- At the method level, a novel task-specific class detection strategy and a novel class-specific prompt generation strategy are proposed to employ SAM for both new and previous tasks. Our method effectively integrates new classes while preserving prior knowledge.

- Our method effectively balances old knowledge retention with new knowledge learning and yields significantly improved accuracy and adaptability, demonstrating superior CSS performance across a diverse range of challenging CSS tasks (see representative results in Figure 1b).

## 2. Related Work

**Continual Semantic Segmentation** The challenges in CSS include catastrophic forgetting, stability-plasticity dilemma, and semantic (background) shift [63]. PLOP [13] employs pseudo-labels generated by the prior model and multi-scale local distillation to preserve old knowledge. A series of works [6, 34, 40, 54, 67, 68] follow this way, aiming to enhance model stability by reducing information loss and preserving existing knowledge. For example, BalCompa [8] selectively distills the most relevant feature, and Cs<sup>2</sup>KCA [11] uses pixel-level features as a prototype for each class. Though Exemplar Replay [49, 52] has advanced significantly in CSS from three aspects: Sample Replay [7, 22, 31, 38, 61], Feature Replay [26, 42, 56, 59] and Auxiliary Data [29, 57], dynamic networks [1, 20, 24, 46, 50, 53, 55] stand out for their efficacy in preserving crucial parameters and enabling flexible task-specific adjustments [15], making them particularly advantageous in CSS. While recent CSS methods like CoMasTRe [15] and CoMFormer [6] based on Mask2Former [10] also explore decoupling strategies, with CoMasTRe focusing on objectness learning and classification separately, our framework follows a distinct detection-then-segmentation paradigm which shows superior performance.

**Language-Driven Continual Learning** Inspired by the observation that humans effectively acquire new visual knowledge through language and motivated by the broad applications of pre-trained vision-language models (VLMs) [18, 37], previous studies have explored VLMs in continual learning classification tasks [21, 65, 69]. However, applications of VLMs for Continual Semantic Segmentation (CSS) are much less explored, primarily because the dense annotations required for segmentation cannot be directly leveraged by these models; only a few studies have explored their potential in Weakly Supervised Continual Semantic Segmentation [58]. To our best knowledge, our work is the first to leverage VLMs in dense-annotated CSS.

## 3. Method

This study focuses on class-incremental semantic segmentation (CISS), where a model learns a sequence of  $T$  semantic segmentation tasks. In the  $t$ -th task ( $t = 1, 2, \dots, T$ ), the model is updated to learn to segment each image of the task into regions of  $c_t$  new foreground classes and a background class, while preserving the ability to segment regions corresponding to the previously learned  $c_1 + c_2 + \dots + c_{t-1}$

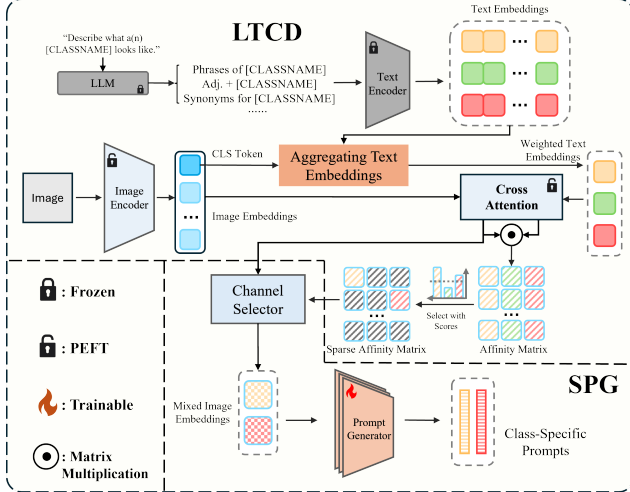


Figure 2. Workflow of the LTCD and SPG module.

classes. In each training image of task  $t$ , the background may contain objects of both previously learned foreground classes (from tasks 1 to  $t-1$ ) and future classes (from tasks  $t+1$  to  $T$ ); this overlapped setting in CISS is more challenging than the disjoint scenario where future classes are absent during learning task  $t$ . After learning task  $t$ , the model is expected to segment any test image containing any subset of the  $c_1 + c_2 + \dots + c_t$  learned classes.

### 3.1. Framework Overview

The proposed CSS framework (Figure 2) is developed based on the insight that the process of segmenting an image can be decoupled into two independent stages, the existence detection of foreground classes in the image (Stage-I) and the accurate delineation of the foreground region(s) for each detected class (Stage-II). With more and more segmentation tasks learned, Stage-I should be able to detect existence of more and more classes. To achieve this goal, a novel language-driven and task-aware class detection (LTCD) module built on pre-trained large language and vision models is designed. This module can find existence of classes for each learned task with the help of task-specific adapters and a detection, and thus catastrophic forgetting of old knowledge for class detection is avoided.

For Stage-II, inspired by the class-agnostic segmentation capability of the recently developed foundation segmentation model SAM, we employ the pre-trained SAM to automatically annotate the region of each detected class. The challenge here is to provide location-relevant prompts informing SAM where to segment for each detected class. To solve this challenge, a segmentation prompt generation (SPG) module is designed to activate SAM for accurate region segmentation of each detected class. The SPG module bridges the LTCD and the CAS modules, taking the patch-level visual embeddings and language-guided class-

wise image embeddings from the LTCD module as input.

In this framework, task-wise continual learning in the LTCD module and class-wise continual learning in the SPG module are responsible to continually learn knowledge of new classes, while the class-agnostic CAS module is responsible for accurate region annotation given location-relevant prompts. By isolating class detection from class-agnostic region annotation, our method provides a robust, modular solution for continual semantic segmentation.

### 3.2. Language-driven Task-aware Class Detection

Suppose the model will be learning the  $t$ -th task including  $c_t$  new classes. The LTCD module utilizes textual prior knowledge of each class in task  $t$  to help adapt the pre-trained image encoder and the cross attention part for task  $t$ . In particular, the encoded textual prior is used in the text-image cross attention blocks to help extract the class-specific visual embedding from the adapted image encoder for rough class awareness. Note that only the task-specific adapters which are added to the pre-trained image encoder and the pre-trained text-image cross attention block are learnable.

#### 3.2.1. Text Encoding

For each of the  $c_t$  classes, a number of  $M + 1$  descriptive phrases are generated (see Section B.1 for the complete template and process). Among them,  $M$  phrases are generated by the large language model [33] using a pre-defined prompt [2, 35]. Unlike conventional approaches that generate complete sentences with redundant linguistic elements, our method employs concise phrasal descriptions (e.g., adjective + class name) to capture essential visual attributes. This focused representation enhances feature distinctiveness and improves class discrimination capabilities. Each phrase is then sent to a pre-trained text encoder to obtain the corresponding text embedding. Consequently, for the  $k$ -th class ( $k = 1, 2, \dots, c_t$ ), a set of  $M + 1$  text embeddings  $\{g_{k,1}, g_{k,2}, \dots, g_{k,M+1}\}$  are generated. The purpose of generating multiple versions of textual descriptions and corresponding text embeddings for each class is to increase diversity and enhance the robustness of the subsequent aggregation step.

*Aggregating text embeddings.* While using multiple textual embeddings enriches class representations by providing a wealth of contextual information, it simultaneously introduces irrelevant or misaligned semantics that do not correspond to the specific content of the input image. To mitigate this issue, we propose an adaptive re-weighting strategy that adjusts the influence of each text embedding based on its relevance to the visual content of the current input image. For an input image  $\mathbf{x}_i$ , the weight for each text embedding is

$$\alpha_{i,k,m} = \frac{\exp(s_{i,k,m})}{\sum_{j=1}^{M+1} \exp(s_{i,k,j})}, \quad (1)$$

where  $m \in \{1, 2, \dots, M+1\}$ ,  $k \in \{1, 2, \dots, c_t\}$ , and the score  $s_{i,k,j} = \cos(\mathbf{V}_i^{cls}, \mathbf{g}_{k,j})$  measures the cosine similarity between the *cls* token of visual embedding  $\mathbf{V}_i$  for the input image  $\mathbf{x}_i$  from the adapted image encoder (see following subsection) and the  $j$ -th text embedding  $\mathbf{g}_{k,j}$  of class  $k$ . The final text embedding for class  $k$  is generated based on weighted sum of all  $M+1$  text embeddings, *i.e.*,

$$\mathbf{e}_{i,k} = \sum_{m=1}^{M+1} \alpha_{i,k,m} \cdot \mathbf{g}_{k,m}. \quad (2)$$

Note that  $\mathbf{e}_{i,k}$  is image-wise, *i.e.*, different input images would lead to different text embeddings  $\mathbf{e}_{i,k}$  for same class  $k$ . The set of text embeddings  $\mathbf{E}_i = [\mathbf{e}_{i,1}, \mathbf{e}_{i,2}, \dots, \mathbf{e}_{i,c_t}] \in \mathbb{R}^{c_t \times d}$  for the  $c_t$  classes of task  $t$  will be utilized along with the visual embedding of input image  $\mathbf{x}_i$  (see below) for language-driven class detection.

### 3.2.2. Task-Specific LoRAs

In our framework, we initialize the pre-trained image encoder (with a Swin Transformer backbone) and cross-attention module from Grounding DINO [27] which are endowed with robust feature extraction and cross-modal alignment capabilities. However, while these pre-trained components provide reliable general representations, they are not specifically optimized for the nuanced requirements of learning novel classes incrementally.

Here, task-specific LoRA [17] adapters are added into both the image encoder and the cross-attention module to learn each new segmentation task. For the image encoder, these lightweight adapters are embedded in each self-attention layer, enhancing discriminative feature extraction for new classes while maintaining the output structure as  $\mathbf{V}_i \in \mathbb{R}^{N \times d}$  for each input image  $\mathbf{x}_i$ , where  $N$  represents visual tokens and  $d$  is the embedding dimension. In the cross-attention module, which coordinates bidirectional information flow between modalities, LoRA adapters are incorporated in the linear projections that generate attention ‘keys’ and ‘values’. This approach enables effective text-guided visual feature optimization through multiple interaction layers, producing enhanced representations  $\mathbf{V}'_i \in \mathbb{R}^{N \times d}$  and  $\mathbf{E}'_i \in \mathbb{R}^{c_t \times d}$  that better capture cross-modal relationships while maintaining computational efficiency.

Note that the learnable adapters are task-specific, which prevents negative transfer and catastrophic forgetting across incremental tasks. All learned adapters for previous tasks  $1$  to  $t-1$  are preserved but not utilized when the model learns task  $t$ . However, during model inference, adapters of each learned task will be utilized to segment any test image.

### 3.2.3. Semantic Alignment and Token Selection

This section details the process of establishing precise semantic correspondence between image regions and class

concepts, a crucial step for class-aware segmentation. While the cross-attention module (described above) refines visual and textual embeddings ( $\mathbf{V}'_i$  and  $\mathbf{E}'_i$  respectively), an explicit alignment measure is needed to guide the segmentation process.

*Affinity matrix construction.* To quantify the alignment between visual tokens and textual class embeddings, we compute an affinity matrix,  $\mathbf{S}_i$ , for each image  $\mathbf{x}_i$ . This matrix represents the pairwise similarity between each visual token and each class embedding, computed as follows

$$\mathbf{S}_i = \cos(\mathbf{V}'_i, \mathbf{E}'_i^T) \in \mathbb{R}^{N \times c_t}, \quad (3)$$

where  $\cos(\cdot, \cdot)$  denotes the cosine similarity measurement. The resulting  $\mathbf{S}_i$  is a matrix where each element  $\mathbf{S}_i[n, k]$  represents the alignment score (dot product) between the  $n$ -th visual token and the  $k$ -th class embedding. Higher values indicate stronger alignment.

*Thresholding for salient token selection.* Some image regions may be irrelevant to learned classes, *e.g.*, background regions in images. To filter out these non-salient regions and focus on the most relevant visual tokens, we apply a thresholding operation to the affinity matrix  $\mathbf{S}_i$ , creating a sparse affinity matrix  $\mathbf{S}'_i$

$$\mathbf{S}'_i[n, k] = \begin{cases} \mathbf{S}_i[n, k], & \text{if } \mathbf{S}_i[n, k] \geq \tau \\ 0, & \text{otherwise} \end{cases} \quad (4)$$

where  $\tau$  is a pre-defined threshold. This operation effectively eliminates weak associations, retaining only visual tokens with strong alignment to at least one class. This sparsity reduces noise and computational cost in subsequent steps.

*Selection of semantically aligned tokens.* From the sparse affinity matrix  $\mathbf{S}'_i$ , we select the visual tokens that exhibit strong alignment with any class. The selection process is defined as follows:

Identify relevant rows: We identify the rows in  $\mathbf{S}'_i$  that contain at least one nonzero element. The collection of these rows corresponds to visual tokens of interest, denoted  $\mathcal{I}_{row}$ . Extract selected tokens: We extract the visual embeddings corresponding to the selected row indices. This forms the set of selected visual embeddings:  $\mathbf{V}'_{i,sel} = \{\mathbf{V}'_i[n, :] | n \in \mathcal{I}_{row}\}$ .

Determine semantic associations: For each selected token in  $\mathbf{V}'_{i,sel}$ , we determine its associated class by identifying the class with the highest alignment score in the corresponding row of the sparse affinity matrix  $\mathbf{S}'_i$ . This is represented by the set of index pairs in the form of (selected token, class), *i.e.*,  $\mathbf{C}_i = \{(n, k) | n \in \mathcal{I}_{row}, k = \arg \max_j \mathbf{S}'_i[n, j]\}$ .

### 3.3. Class-Specific Prompt Generation

This section describes the generation of class-specific positional prompts from the selected visual embedding ( $\mathbf{V}'_{i,sel}$ ),

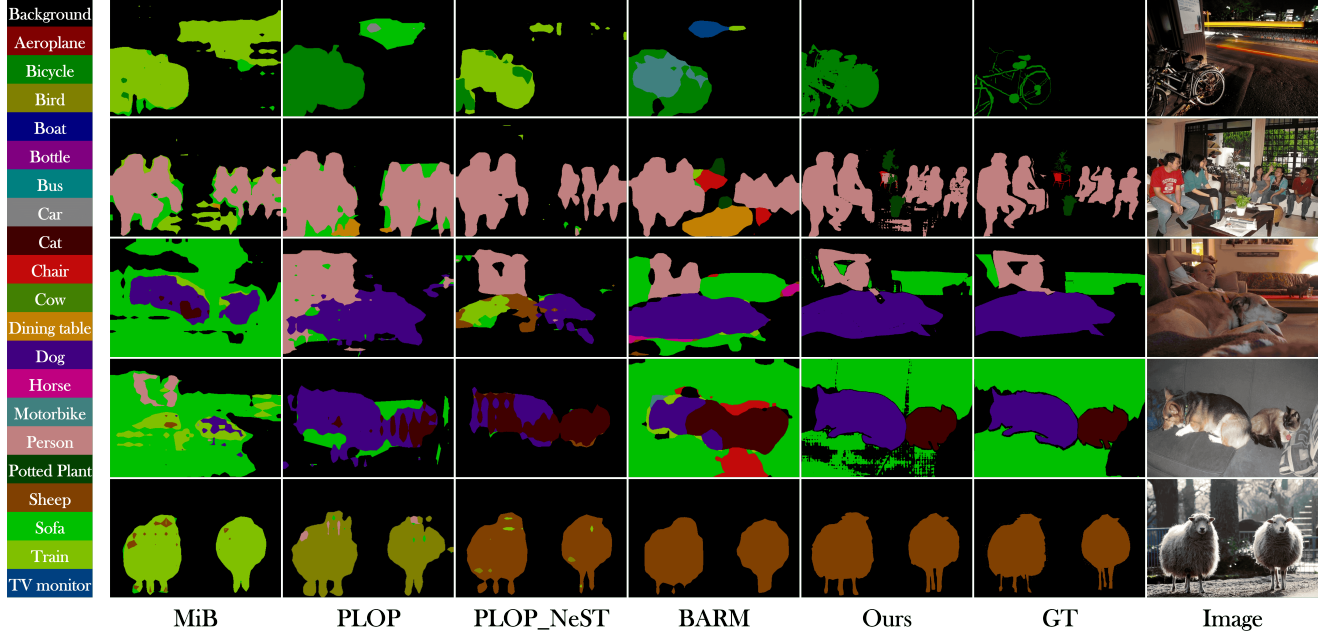


Figure 3. The visualization comparison from the last task on the Pascal VOC2012 10-1 setting.

which are then used for class-agnostic segmentation. We propose a Segmentation Prompt Generation module which employs class-specific generators, isolating the prompt generation process for each class. This design approach confers significant architectural advantages when compared to conventional CSS methods. Traditional CSS approaches typically formulate segmentation as a pixel-level multi-class classification problem, wherein decision boundaries must be continuously calibrated to accommodate previously learned classes. Such recalibration inevitably leads to **error accumulation** across sequential tasks. By decoupling the prompt generation process for each class, we effectively isolate the learning of class-specific features, preventing interference between classes during continual learning.

### 3.3.1. Channel Selection

The Channel Selector organizes the selected visual embeddings,  $\mathbf{V}_i^{\text{sel}}$ , based on their semantic associations,  $\mathbf{C}_i$  (defined previously). For each class  $k$ , it extracts the token embeddings most strongly associated with that class. Formally, the class-specific token set,  $\mathcal{T}_k$ , is defined as  $\mathcal{T}_k = \{\mathbf{V}_i^{\text{sel}}[n, :] | (n, j) \in \mathbf{C}_i, j = k\}$ .

### 3.3.2. Prompt Generation (pGen)

To create a consistent input dimension for our prompt generator, we process these class-specific tokens as follows using a max token length  $Q_m$  for every class, i.e.,  $\hat{\mathbf{z}}_k = \text{Flatten}(\mathcal{T}_k) \oplus \mathbf{L}_k$ , where  $\text{Flatten}(\cdot)$  concatenates all tokens in  $\mathcal{T}_k$  into a single vector and then adjusts the length to a fixed size  $Q_m$  by either padding with zeros or truncating.

$\mathbf{L}_k$  is a learnable class-specific embedding, and  $\oplus$  denotes element-wise addition. The resulting vector  $\hat{\mathbf{z}}_k$  has a fixed dimension  $d_z$ . By generating prompts specific to each class, *pGen could capture the unique segmentation characteristics of different classes*, which often exhibit distinct mask patterns and boundaries. This tailored prompt generation enhances the decoder’s performance, enabling more precise segmentation across diverse object categories. The final step involves transforming this class-specific representation into positional prompts for SAM. This is formulated as  $\mathbf{p}_k = \text{pGen}_k(\hat{\mathbf{z}}_k)$ , where  $\text{pGen}_k$  is a class-specific two-layer MLP dedicated to class  $k$ , and  $\mathbf{P}_k \in \mathbb{R}^{m \times d_p}$  represents  $m$  prompt tokens with dimension  $d_p$  (in our implementation,  $m = 6$ ).

### 3.4. Class-Agnostic Segmentation and Aggregation

The Class-Agnostic Segmentation (CAS) module utilizes a segmentation foundation model, and we currently employ SAM (Segment Anything Model) [23] for this role. SAM works in a class-agnostic manner and can generate high-quality segmentation results for the input image solely based on spatial prompt conditions. Specifically, for each class-specific prompt  $\mathbf{p}_k$  (from above section), SAM outputs a corresponding mask  $\mathcal{M}_k$  and a confidence score. These individual class-specific masks are aggregated into a final semantic segmentation map.

It is worth noting that the CAS module is frozen in the whole continual learning process. However, when the model learns task  $t$ , the outputs from CAS are used to gen-

Table 1. Comparison with existing methods on PASCAL VOC2012 in mIoU (%). The 1<sup>st</sup> highest results among Replay methods and the 1<sup>st</sup> highest results among Data-free methods (excluding our method) are marked with underline. † means the latest methods proposed from 2024 to 2025. \* is on behalf of our own implementation.

	Method	19-1 (2 tasks)			15-5 (2 tasks)			15-1 (6 tasks)			10-1 (11 tasks)		
		0-19	20	all	0-15	16-20	all	0-15	16-20	all	0-10	11-20	all
Replay	MicroSeg-M [66]	—	—	—	82.9	60.1	77.5	82.0	47.3	73.3	78.9	59.2	70.1
	SSUL-M [7]	<u>77.38</u>	22.43	<u>74.76</u>	79.3	55.1	73.5	78.8	49.7	71.9	75.3	54.1	65.2
	RECALL [31]	67.9	<u>53.5</u>	68.4	66.6	50.9	64.0	65.7	47.8	62.7	59.5	46.7	54.8
	SATS-M [36]	—	—	—	81.44	70.02	78.72	80.37	64.54	76.61	76.21	61.62	69.27
	IPSeg-M† [60]	—	—	—	<u>83.3</u>	<u>73.3</u>	<u>80.9</u>	<u>83.5</u>	<u>75.1</u>	<u>81.5</u>	<u>80.3</u>	<u>76.7</u>	<u>78.6</u>
Data-free	MiB* [4]	69.91	20.63	67.45	75.48	49.41	68.47	36.71	12.12	30.82	12.20	13.19	12.61
	PLOP* [13]	74.15	35.58	72.04	75.49	49.66	69.34	64.09	20.12	53.11	44.03	15.51	30.45
	MiB+NeST†* [51]	70.25	26.06	68.91	75.46	48.68	69.47	60.24	19.97	48.97	52.36	21.07	37.41
	PLOP+NeST†* [51]	76.09	47.93	73.82	76.11	48.47	68.44	48.97	23.28	48.18	54.21	17.83	36.91
	MicroSeg [66]	—	—	—	81.9	54.0	75.2	80.5	40.8	71.0	73.5	53.0	63.8
	CoMFormer [6]	75.35	24.06	72.91	74.68	54.30	71.12	70.78	32.24	61.60	—	—	—
	CoMasTRe† [15]	75.13	<u>69.51</u>	<u>74.86</u>	79.73	51.93	73.11	69.77	43.62	63.54	—	—	—
	IPSeg [60]	—	—	—	<u>81.4</u>	<u>62.4</u>	<u>76.9</u>	<u>82.4</u>	52.9	<u>75.4</u>	<u>80.0</u>	<u>61.2</u>	<u>71.0</u>
	SATS* [36]	77.42	61.07	74.41	80.24	61.17	75.70	78.38	<u>62.02</u>	74.48	64.27	58.66	61.60
	BARM†* [64]	<u>77.6</u>	41.4	75.2	—	—	—	77.3	45.8	69.8	72.2	49.8	61.9
	SSUL [7]	—	—	—	79.7	55.3	73.9	78.1	33.4	67.5	74.3	51.0	63.2
	<b>Ours</b>	<b>82.92</b>	<b>83.71</b>	<b>83.95</b>	<b>84.03</b>	<b>81.68</b>	<b>83.47</b>	<b>83.81</b>	<b>82.12</b>	<b>83.40</b>	<b>84.03</b>	<b>82.12</b>	<b>83.12</b>

erate the segmentation loss function. In our framework, the same segmentation loss as that for SAM training is adopted to train the learnable class-specific prompt generators, and the loss is also used together with the asymmetric loss [39] to train the task-specific LoRAs in the LTCD module.

During model inference, given a test image, the task-specific and class-specific components of each task are plugged into the segmentation system to segment image regions specifically for those classes estimated appearing in the input image. Such inference process is run over all tasks and the results are collected for the final segmentation. The final segmentation is created by aggregating individual class masks. While pixel ownership is unambiguous for the vast majority of pixels, any rare spatial overlaps are resolved using a confidence-based approach. The pixel is assigned to the class with the highest confidence score from the SAM decoder. Notably, this process requires no task ID, with time linear complexity with respect to the number of learned tasks  $T$ . Since only one adapter resides in memory at any time, maximum memory usage remains identical to that in single-task models. For time-sensitive applications, memory-time tradeoff techniques [41] can be used to reduce inference latency.

## 4. Experiments

### 4.1. Experimental Setup

**Datasets** Following previous studies [4, 13], we evaluate our method on PASCAL VOC2012 [14] and ADE20K [70]. PASCAL VOC2012 contains 20 object classes while ADE20K presents a more challenging scenario with 150 classes. Dataset statistics are in Appendix C.

**CSS Settings.** The training process is divided into  $T$  tasks with certain protocol. The *overlapped* protocol, which is more challenging and realistic compared to the *disjoint* setting, allows images to contain old classes previously learned and future classes to be learned [36]. For these images, annotations are provided only for the current task’s classes and image regions corresponding to both old and future classes are annotated as background. Our experiments use this *overlapped* setting throughout. For instance, in the VOC2012 10-1 (11 tasks) setting, the model first learns to segment 10 classes, then incrementally learns one new class in each of 10 new tasks.

**Implementation details.** The model was trained for 5 epochs on PASCAL VOC2012 and 20 epochs on ADE20K using AdamW [28] optimizer (initial learning rate  $1 \times 10^{-4}$ , weight decay 0.05) with a polynomial learning rate schedule. For the LTCD module, we set the similarity threshold  $\tau$  to 0.3 for PASCAL VOC2012 and 0.2 for ADE20K, ensuring an appropriate quantity of selected visual tokens in  $\mathbf{V}_i^{\text{sel}}$ , with  $M = 30$  descriptive phrases per class and LoRA rank  $L = 32$ . The SPG module uses  $m = 6$  prompt tokens with a single hidden layer, and pGen input lengths of 512 and 1024 for PASCAL VOC2012 and ADE20K respectively, with the longer length for ADE20K accommodating its complex scene composition and higher object density. All experiments were conducted with batch size 24 on 8 NVIDIA 3090 GPUs.

### 4.2. Main Results

Tabs. 1 and 2 present the evaluation results of the proposed method on PASCAL VOC2012 and ADE20K. On

Table 2. Comparison with existing methods on ADE20K in mIoU (%). The 1<sup>st</sup> highest results among Replay methods and the 1<sup>st</sup> highest results among Data-free methods (excluding our method) are marked with underline. † means the latest methods proposed from 2024 to 2025. \* is on behalf of our own implementation.

	Method	100-50 (2 tasks)			100-10 (6 tasks)			100-5 (11 tasks)		
		0-100	101-150	all	0-100	101-150	all	0-100	101-150	all
Replay	IPSeg-M† [60]	43.8	31.5	39.7	43.0	30.9	39.0	43.2	30.4	38.9
	SSUL-M [7]	41.5	<u>48.0</u>	33.7	41.6	19.9	34.4	41.6	20.1	34.5
	TIKP† [62]	42.2	20.2	34.9	41.0	19.6	33.8	37.5	17.6	30.9
Data-free	MiB* [4]	39.02	16.73	31.29	36.68	9.81	27.77	34.22	5.26	24.29
	PLOP* [13]	40.38	13.41	31.52	39.46	12.58	30.10	38.12	7.32	27.39
	MiB+NeST†* [51]	38.84	23.11	33.55	38.79	19.10	32.24	38.39	17.46	31.23
	PLOP+NeST†* [51]	40.78	22.78	34.84	39.42	20.50	33.21	37.83	16.89	30.53
	CoMFormer [6]	44.70	26.20	38.40	40.60	15.60	32.30	39.50	13.60	30.90
	CoMasTRe† [15]	45.73	26.02	39.20	42.32	18.42	34.41	40.82	15.83	32.55
	BARM†* [64]	42.0	23.0	35.7	41.1	23.1	35.2	40.5	21.2	34.1
	BalConpas-R† [8]	<u>50.8</u>	<u>30.4</u>	<u>44.0</u>	<u>48.1</u>	25.3	<u>40.5</u>	<u>43.9</u>	22.7	36.9
	IPSeg† [60]	43.2	29.0	38.4	42.5	<u>27.8</u>	37.6	43.1	<u>26.2</u>	<u>37.6</u>
	SSUL [7]	41.9	20.1	34.6	40.7	19.0	33.5	41.3	16.0	32.9
	<b>Ours</b>	<b>57.72</b>	<b>51.21</b>	<b>56.80</b>	<b>58.19</b>	<b>52.03</b>	<b>56.92</b>	<b>57.53</b>	<b>55.62</b>	<b>56.89</b>

VOC2012, our method achieves the best performance across all the four common CSS splitting settings, with 83.12% in the challenging 10-1 setting, surpassing the previous SOTA method IPSeg (using data replay strategy) by a significant margin of 4.52%. The visual examples in Fig. 3 show that our method has good mask quality while maintaining resilience to semantic shift and catastrophic forgetting. It can be clearly seen from Fig. 4 that the existing methods have obvious limitations in the process of incremental learning. It is particularly noteworthy that these methods, in the last few steps of the Pascal VOC 2012 15-1 setup, are primarily concerned with preventing forgetting of previously learned categories rather than effectively learning newly introduced categories. As the figure shows, other methods(PLOP and PLOP NeST) do not perform well in learning new categories ( such as TV Monitor for case b ). This is a direct reflection of their design and training philosophy - too much emphasis on preventing catastrophic forgetting and too little on the effective absorption of new knowledge. In case a, we can see method misclassify sofa into previously learned categories after task 4. Our proposed method can not only maintain accurate recognition of previous categories, but also efficiently learn and segment newly introduced categories. Similarly on the more challenging ADE20K dataset, our method also excels in all the 100-50, 100-10 and 100-5 settings. Notably, our method significantly outperforms the SOTA method with a 17.99% mIoU increase in the 100-5 setting. These results demonstrate its strong performance in learning new knowledge while preserving old knowledge.

Furthermore, in the more challenging CSS settings where the number of classes learned in the first task is the

Table 3. Quantitative comparison of different methods for challenging settings: 2-2, 4-2, and 4-4 incremental segmentation scenarios on PASCAL VOC 2012.

Method	2-2 (10 tasks)			4-2 (9 tasks)			4-4 (5 tasks)		
	0-2	3-20	all	0-4	5-20	all	0-4	5-20	all
MiB [4]	3.27	6.35	5.91	7.08	6.72	6.80	39.50	20.07	24.70
PLOP [13]	24.96	5.38	8.18	15.41	6.55	8.67	28.54	15.95	18.95
MiB+NeST [51]	13.44	6.72	7.68	10.09	7.51	7.77	38.31	21.3	25.35
PLOP+NeST [51]	27.98	6.53	8.26	17.57	7.84	10.15	33.89	17.84	21.66
<b>Ours</b>	<b>87.31</b>	<b>82.52</b>	<b>83.20</b>	<b>87.63</b>	<b>82.22</b>	<b>83.50</b>	<b>87.63</b>	<b>81.31</b>	<b>82.81</b>

Table 4. Ablation study on PASCAL VOC2012, evaluated in terms of mIoU (%). The components include LoRA (L), Class-specific pGen (CG), and semantic aggregation (S).

Components	19-1 (2 tasks)			10-1 (11 tasks)			15-1 (6 tasks)					
	L	CG	S	0-19	20	all	0-10	11-20	all	0-15	16-20	all
✗	✗	✗		25.16	62.79	26.95	22.32	25.81	23.98	25.42	26.28	25.62
✓	✓	✗		79.37	80.26	79.41	81.22	80.51	80.88	80.35	80.82	80.46
✓	✗	✓		29.54	77.41	31.81	28.76	27.43	27.89	30.14	28.17	28.83
✗	✓	✓		76.13	77.97	76.21	77.64	76.33	77.01	78.38	77.12	78.03
✓	✓	✓		82.92	83.71	83.95	84.03	82.12	83.12	83.81	82.12	83.40

same as that in each subsequent task, including the settings 2-2 (10 tasks), 4-2 (9 tasks), and 4-4 (5 tasks), the superiority of our method becomes more evident. As shown in Fig. 1b and Tab. 3, our method consistently maintained both plasticity and stability in these highly challenging scenarios, outperforming competing methods by huge gaps of 74.94%, 73.35%, and 57.46% respectively.

### 4.3. Ablation Studies

Ablation studies were performed to verify the validity of three key components in our framework: LoRA, pGen, and semantic aggregation. As shown in Tab. 4, removing each of three components leads to worse performance in all task settings. In addition, when class-specific pGen was replaced by classes-shared pGen, a dramatic drop particularly in 10-

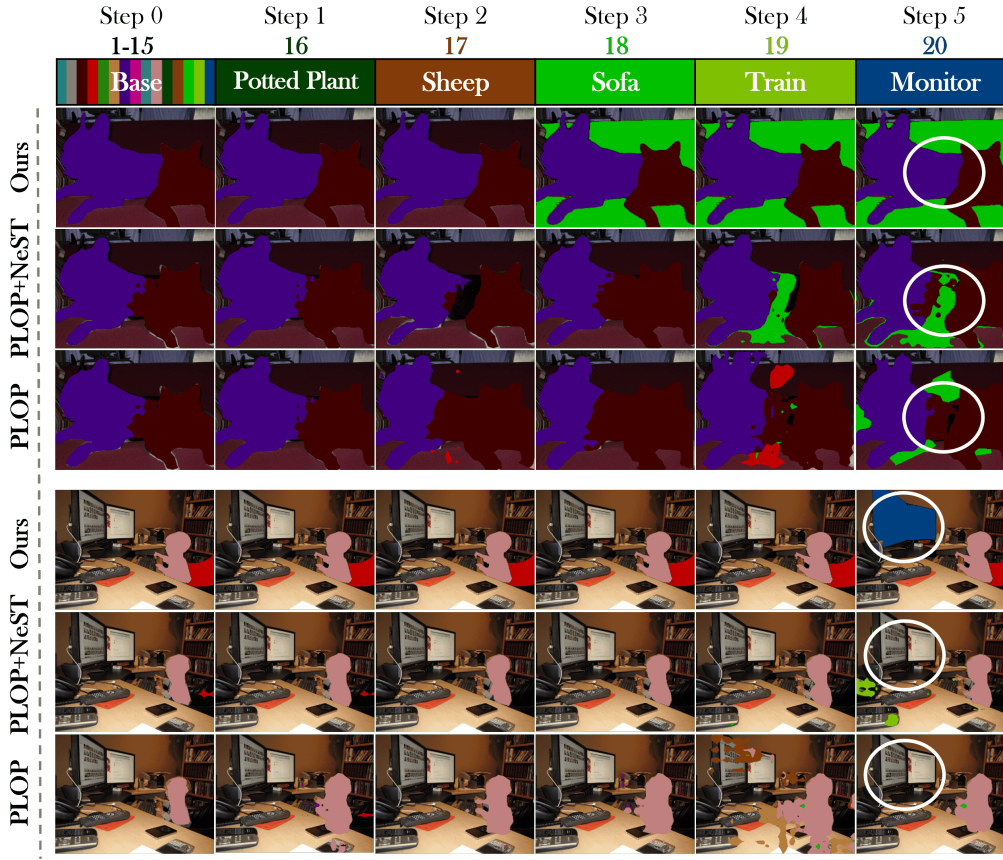


Figure 4. The visualization comparison from the last task on the Pascal VOC 2012 15-1 setting. We demonstrate our ability to resist forgetting and learn new categories

1 and 15-1 settings was observed. This drop happened because, with the shared pGen, the system had to adjust for each new class during training, as shown by the images in Fig. A3. All these results confirm the necessity of the proposed components in our framework.

#### 4.4. Sensitivity Studies

The sensitivity of our method to hyper-parameter choice is also evaluated. As demonstrated in Fig. 5, when varying the LoRA ranks within the range [16, 64], the number of hidden layers in the class-specific pGen module within the range [0, 2], the number of textual descriptions for each class based on the LLM within the range [1, 51], our method performs stably well and always better than the representative strong baseline, supporting the robustness of our method to hyper-parameter choice.

#### 4.5. Additional Studies

Additional experiments demonstrate that simply incorporating powerful foundation models like SAM is insufficient for effective CSS, and that the proposed class-specific prompt generation in our method is necessary.

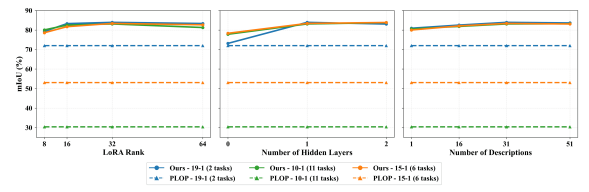


Figure 5. Sensitivity study on PASCAL VOC2012.

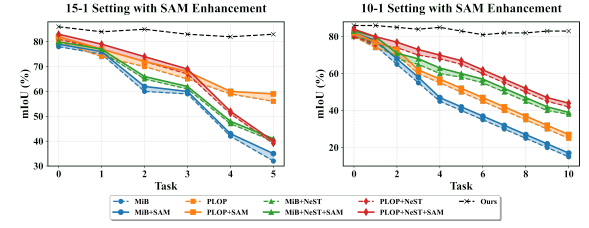


Figure 6. Segmentation performance on PASCAL VOC2012 with and without SAM enhancement.

As shown in Fig. 6, simply applying SAM as a post-processing module to existing CSS methods yields only marginal improvements, with less than 6% mIoU across various settings. This limited gain reveals fundamental

limitations when SAM is applied directly to CSS outputs: blurred edges in CSS predictions compromise SAM’s segmentation capabilities, and SAM’s class-agnostic nature cannot correct semantic inconsistencies inherent in CSS outputs. In contrast, our method with the proposed prompt generation module which generates precise class-aware positional embeddings overcomes these limitations by intelligently guiding SAM to produce refined segmentation masks.

To further confirm the efficacy of the proposed prompt generation module, ground-truth class existence information and bounding box for each class region were first obtained for each test image by Grounding DINO. These boxes were then used as spatial prompts for SAM to produce segmentation masks. Such approach achieves 84% mIoU on PASCAL VOC2012 and 57% mIoU on ADE20K. While this performance is comparable to our method (83% on VOC2012 and 56% on ADE20K), it is important to note that our approach achieves this without requiring ground-truth tags during inference and operates under the challenging constraints of continual learning. This demonstrates that our class-specific prompt generation approach effectively bridges detection and segmentation in CSS scenarios, achieving near-optimal performance even without perfect class knowledge.

Finally, we analyse the computational cost of our approach. Similar to previous continual learning studies which employ task-specific modules [25], our method introduces computational overhead during inference primarily from switching task-specific LoRA parameters. The inference time for a single task is 0.3 second per image, and the full process for six tasks in the (15-1) setting takes about 1.9 seconds per image. In comparison, most existing single encoder-decoder based CSS methods takes around 0.5 second per image. Despite leveraging foundation models, our parameter growth remains highly manageable. Each class requires only 8MB for the pGen module (0.225% of total model size), while all tasks’ LoRA adapters collectively need merely 22.18MB (0.62% of total model size). Each task requires relatively few trainable parameters per increment [19], yet achieves state-of-the-art performance with remarkable gains in challenging settings, demonstrating practical applicability comparable to offline-trained models. Given our method’s substantial performance gains and affordable storage overhead, this trade-off is well-justified for non-realtime applications.

## 5. Conclusion

In this work, we propose a two-stage framework for Continual Semantic Segmentation (CSS) that decouples class-aware detection from class-agnostic segmentation. Our method achieves state-of-the-art performance across various CSS tasks. The superior performance stems from task-

specific modeling with conflict-free formulation. By leveraging pre-trained text and image encoders, this study provides a practical solution for real-world applications such as autonomous driving and medical imaging, offering a scalable path for CSS. The main limitation of our method is the inference time due to the sequential switching of task-specific parameters. Future work could explore parameter merging techniques to address this scalability issue.

## References

- [1] Donghyeon Baek, Youngmin Oh, Sanghoon Lee, Junghyun Lee, and Bumsub Ham. Decomposed knowledge distillation for class-incremental semantic segmentation. *Advances in Neural Information Processing Systems*, 35:10380–10392, 2022. [2](#)
- [2] Xiaoyu Bai and Yong Xia. Sam++: Enhancing anatomic matching using semantic information and structural inference. 2023. [3](#)
- [3] Elena Camuffo and Simone Milani. Continual learning for lidar semantic segmentation: Class-incremental and coarse-to-fine strategies on sparse data. In *2023 IEEE/CVF Conference on Computer Vision and Pattern Recognition Workshops (CVPRW)*, pages 2447–2456, 2023. [1](#)
- [4] Fabio Cermelli, Massimiliano Mancini, Samuel Rota Bulò, Elisa Ricci, and Barbara Caputo. Modeling the background for incremental learning in semantic segmentation. *2020 IEEE/CVF Conference on Computer Vision and Pattern Recognition (CVPR)*, pages 9230–9239, 2020. [1, 6, 7](#)
- [5] Fabio Cermelli, Massimiliano Mancini, Samuel Rota Bulo, Elisa Ricci, and Barbara Caputo. Modeling the Background for Incremental Learning in Semantic Segmentation. In *CVPR*, 2020. [1](#)
- [6] Fabio Cermelli, Matthieu Cord, and Arthur Douillard. CoFormer: Continual Learning in Semantic and Panoptic Segmentation. In *CVPR*, 2023. [2, 6, 7](#)
- [7] Sungmin Cha, YoungJoon Yoo, Taesup Moon, et al. Ssul: Semantic segmentation with unknown label for exemplar-based class-incremental learning. *Advances in neural information processing systems*, 34:10919–10930, 2021. [2, 6, 7](#)
- [8] Jinpeng Chen, Runmin Cong, Yuxuan Luo, Horace Ho-Shing Ip, and Sam Kwong. Strike a balance in continual panoptic segmentation. *ECCV*, 2024. [2, 7](#)
- [9] Liang-Chieh Chen. Rethinking atrous convolution for semantic image segmentation. *arXiv preprint arXiv:1706.05587*, 2017. [2](#)
- [10] Bowen Cheng, Ishan Misra, Alexander G Schwing, Alexander Kirillov, and Rohit Girdhar. Masked-attention mask transformer for universal image segmentation. In *Proceedings of the IEEE/CVF conference on computer vision and pattern recognition*, pages 1290–1299, 2022. [2](#)
- [11] Wei Cong, Yang Cong, Yuyang Liu, and Gan Sun. Cs2k: Class-specific and class-shared knowledge guidance for incremental semantic segmentation. *ECCV*, abs/2407.09047, 2024. [2](#)
- [12] DeepSeek-AI, Aixin Liu, Bei Feng, Bing Xue, Bingxuan Wang, Bochao Wu, Chengda Lu, Chenggang Zhao, Chengqi

Deng, Chenyu Zhang, Chong Ruan, Damai Dai, Daya Guo, Dejian Yang, Deli Chen, Dongjie Ji, Erhang Li, Fangyun Lin, Fucong Dai, Fuli Luo, Guangbo Hao, Guanting Chen, Guowei Li, H. Zhang, Han Bao, Hanwei Xu, Haocheng Wang, Haowei Zhang, Honghui Ding, Huajian Xin, Huazuo Gao, Hui Li, Hui Qu, J. L. Cai, Jian Liang, Jianzhong Guo, Jiaqi Ni, Jiashi Li, Jiawei Wang, Jin Chen, Jingchang Chen, Jingyang Yuan, Junjie Qiu, Junlong Li, Junxiao Song, Kai Dong, Kai Hu, Kaige Gao, Kang Guan, Kexin Huang, Kuai Yu, Lean Wang, Lecong Zhang, Lei Xu, Leyi Xia, Liang Zhao, Litong Wang, Liyue Zhang, Meng Li, Miaojun Wang, Mingchuan Zhang, Minghua Zhang, Minghui Tang, Mingming Li, Ning Tian, Panpan Huang, Peiyi Wang, Peng Zhang, Qiancheng Wang, Qihao Zhu, Qinyu Chen, Qiushi Du, R. J. Chen, R. L. Jin, Ruiqi Ge, Ruisong Zhang, Ruizhe Pan, Runji Wang, Runxin Xu, Ruoyu Zhang, Ruyi Chen, S. S. Li, Shanghao Lu, Shangyan Zhou, Shanhuang Chen, Shaoqing Wu, Shengfeng Ye, Shengfeng Ye, Shirong Ma, Shiyu Wang, Shuang Zhou, Shuiping Yu, Shunfeng Zhou, Shuting Pan, T. Wang, Tao Yun, Tian Pei, Tianyu Sun, W. L. Xiao, Wangding Zeng, Wanjia Zhao, Wei An, Wen Liu, Wenfeng Liang, Wenjun Gao, Wenqin Yu, Wentao Zhang, X. Q. Li, Xiangyue Jin, Xianzu Wang, Xiao Bi, Xiaodong Liu, Xiaohan Wang, Xiaojin Shen, Xiaokang Chen, Xiaokang Zhang, Xiaosha Chen, Xiaotao Nie, Xiaowen Sun, Xiaoxiang Wang, Xin Cheng, Xin Liu, Xin Xie, Xingchao Liu, Xingkai Yu, Xinnan Song, Xinxia Shan, Xinyi Zhou, Xinyu Yang, Xinyuan Li, Xuecheng Su, Xuheng Lin, Y. K. Li, Y. Q. Wang, Y. X. Wei, Y. X. Zhu, Yang Zhang, Yanhong Xu, Yanhong Xu, Yanping Huang, Yao Li, Yao Zhao, Yaofeng Sun, Yaohui Li, Yaohui Wang, Yi Yu, Yi Zheng, Yichao Zhang, Yifan Shi, Yiliang Xiong, Ying He, Ying Tang, Yishi Piao, Yisong Wang, Yixuan Tan, Yiyang Ma, Yiyuan Liu, Yongqiang Guo, Yu Wu, Yuan Ou, Yuchen Zhu, Yuduan Wang, Yue Gong, Yuheng Zou, Yujia He, Yukun Zha, Yunfan Xiong, Yuxian Ma, Yuting Yan, Yuxiang Luo, Yuxiang You, Yuxuan Liu, Yuyang Zhou, Z. F. Wu, Z. Z. Ren, Zehui Ren, Zhangli Sha, Zhe Fu, Zhean Xu, Zhen Huang, Zhen Zhang, Zhenda Xie, Zhengyan Zhang, Zhewen Hao, Zhibin Gou, Zhicheng Ma, Zhigang Yan, Zhihong Shao, Zhipeng Xu, Zhiyu Wu, Zhongyu Zhang, Zhuoshu Li, Zihui Gu, Zijia Zhu, Zijun Liu, Zilin Li, Ziwei Xie, Ziyang Song, Ziyi Gao, and Zizheng Pan. Deepseek-v3 technical report, 2025. 3

[13] Arthur Douillard, Yifu Chen, Arnaud Dapogny, and Matthieu Cord. PLOP: Learning without Forgetting for Continual Semantic Segmentation. In *CVPR*, 2021. 1, 2, 6, 7

[14] Mark Everingham, Luc Van Gool, Christopher K. I. Williams, John Winn, and Andrew Zisserman. The Pascal Visual Object Classes (VOC) Challenge. *IJCV*, 88(2):303–338, 2010. 6, 3

[15] Yizheng Gong, Siyue Yu, Xiaoyang Wang, and Jimin Xiao. Continual segmentation with disentangled objectness learning and class recognition. In *Proceedings of the IEEE/CVF Conference on Computer Vision and Pattern Recognition*, pages 3848–3857, 2024. 2, 6, 7

[16] Camila González, Georgios Sakas, and A. Mukhopadhyay. What is wrong with continual learning in medical image segmentation? *ArXiv*, abs/2010.11008, 2020. 1

[17] Edward J Hu, Yelong Shen, Phillip Wallis, Zeyuan Allen-Zhu, Yuanzhi Li, Shean Wang, Lu Wang, and Weizhu Chen. Lora: Low-rank adaptation of large language models. *arXiv preprint arXiv:2106.09685*, 2021. 4

[18] Xinyu Huang, Yi-Jie Huang, Youcai Zhang, Weiwei Tian, Rui Feng, Yuejie Zhang, Yanchun Xie, Yaqian Li, and Lei Zhang. Open-set image tagging with multi-grained text supervision. 2023. 2

[19] Zhanghexuan Ji, Dazhou Guo, Puyang Wang, Ke Yan, Le Lu, Minfeng Xu, Qifeng Wang, Jia Ge, Mingchen Gao, Xianghua Ye, and Dakai Jin. Continual segment: Towards a single, unified and non-forgetting continual segmentation model of 143 whole-body organs in ct scans. In *Proceedings of the IEEE/CVF International Conference on Computer Vision (ICCV)*, pages 21140–21151, 2023. 9

[20] Tobias Kalb, Niket Ahuja, Jingxing Zhou, and Jürgen Beyrer. Effects of architectures on continual semantic segmentation. In *2023 IEEE Intelligent Vehicles Symposium (IV)*, pages 1–8. IEEE, 2023. 2

[21] Baoshuo Kan, Teng Wang, Wenpeng Lu, Xiantong Zhen, Weili Guan, and Feng Zheng. Knowledge-aware prompt tuning for generalizable vision-language models. In *Proceedings of the IEEE/CVF International Conference on Computer Vision*, pages 15670–15680, 2023. 2

[22] Jin Kim, Jiyoung Lee, Jungin Park, Dongbo Min, and Kwanghoon Sohn. Pin the memory: Learning to generalize semantic segmentation. In *Proceedings of the IEEE/CVF Conference on Computer Vision and Pattern Recognition*, pages 4350–4360, 2022. 2

[23] Alexander Kirillov, Eric Mintun, Nikhila Ravi, Hanzi Mao, Chloe Rolland, Laura Gustafson, Tete Xiao, Spencer Whitehead, Alexander C Berg, Wan-Yen Lo, et al. Segment anything. In *Proceedings of the IEEE/CVF International Conference on Computer Vision*, pages 4015–4026, 2023. 5

[24] Marvin Klingner, Mouadh Ayache, and Tim Fingscheidt. Continual batchnorm adaptation (cbna) for semantic segmentation. *IEEE Transactions on Intelligent Transportation Systems*, 23(11):20899–20911, 2022. 2

[25] Jiashuo Li, Shaokun Wang, Bo Qian, Yuhang He, Xing Wei, Qiang Wang, and Yihong Gong. Dynamic integration of task-specific adapters for class incremental learning. In *Proceedings of the IEEE/CVF Conference on Computer Vision and Pattern Recognition (CVPR)*, pages 30545–30555, 2025. 9

[26] Jie Liu, Yanqi Bao, Guo-Sen Xie, Huan Xiong, Jan-Jakob Sonke, and Efstratios Gavves. Dynamic prototype convolution network for few-shot semantic segmentation. In *Proceedings of the IEEE/CVF Conference on Computer Vision and Pattern Recognition*, pages 11553–11562, 2022. 2

[27] Shilong Liu, Zhaoyang Zeng, Tianhe Ren, Feng Li, Hao Zhang, Jie Yang, Qing Jiang, Chunyuan Li, Jianwei Yang, Hang Su, Jun Zhu, and Lei Zhang. Grounding dino: Marrying dino with grounded pre-training for open-set object detection, 2024. 4

[28] I Loshchilov. Decoupled weight decay regularization. *arXiv preprint arXiv:1711.05101*, 2017. 6

[29] Andrea Maracani, Umberto Michieli, Marco Toldo, and Pietro Zanuttigh. Recall: Replay-based continual learning in

semantic segmentation. *International Conference on Computer Vision, International Conference on Computer Vision*, 2021. 2

[30] Andrea Maracani, Umberto Micheli, Marco Toldo, and Pietro Zanuttigh. Recall: Replay-based continual learning in semantic segmentation. In *Proceedings of the IEEE/CVF international conference on computer vision*, pages 7026–7035, 2021. 1

[31] Andrea Maracani, Umberto Micheli, Marco Toldo, and Pietro Zanuttigh. Recall: Replay-based continual learning in semantic segmentation. *International Conference on Computer Vision, International Conference on Computer Vision*, 2021. 2, 6

[32] OpenAI, Josh Achiam, Steven Adler, Sandhini Agarwal, Lama Ahmad, Ilge Akkaya, Florencia Leoni Aleman, Diogo Almeida, Janko Altenschmidt, Sam Altman, Shyamal Anadkat, Red Avila, Igor Babuschkin, Suchir Balaji, Valerie Balcom, Paul Baltescu, Haiming Bao, Mohammad Bavarian, Jeff Belgum, Irwan Bello, Jake Berdine, Gabriel Bernadett-Shapiro, Christopher Berner, Lenny Bogdonoff, Oleg Boiko, Madelaine Boyd, Anna-Luisa Brakman, Greg Brockman, Tim Brooks, Miles Brundage, Kevin Button, Trevor Cai, Rosie Campbell, Andrew Cann, Brittany Carey, Chelsea Carlson, Rory Carmichael, Brooke Chan, Che Chang, Fotis Chantzis, Derek Chen, Sully Chen, Ruby Chen, Jason Chen, Mark Chen, Ben Chess, Chester Cho, Casey Chu, Hyung Won Chung, Dave Cummings, Jeremiah Currier, Yunxing Dai, Cory Decareaux, Thomas Degry, Noah Deutsch, Damien Deville, Arka Dhar, David Dohan, Steve Dowling, Sheila Dunning, Adrien Ecoffet, Atty Eleti, Tyna Eloundou, David Farhi, Liam Fedus, Niko Felix, Simón Posada Fishman, Juston Forte, Isabella Fulford, Leo Gao, Elie Georges, Christian Gibson, Vik Goel, Tarun Gogineni, Gabriel Goh, Rapha Gontijo-Lopes, Jonathan Gordon, Morgan Grafstein, Scott Gray, Ryan Greene, Joshua Gross, Shixiang Shane Gu, Yufei Guo, Chris Hallacy, Jesse Han, Jeff Harris, Yuchen He, Mike Heaton, Johannes Heidecke, Chris Hesse, Alan Hickey, Wade Hickey, Peter Hoeschele, Brandon Houghton, Kenny Hsu, Shengli Hu, Xin Hu, Joost Huizinga, Shantanu Jain, Shawn Jain, Joanne Jang, Angela Jiang, Roger Jiang, Haozhun Jin, Denny Jin, Shino Jomoto, Billie Jonn, Heewoo Jun, Tomer Kaftan, Łukasz Kaiser, Ali Kamali, Ingmar Kanitscheider, Nitish Shirish Keskar, Tabarak Khan, Logan Kilpatrick, Jong Wook Kim, Christina Kim, Yongjik Kim, Jan Hendrik Kirchner, Jamie Kiros, Matt Knight, Daniel Kokotajlo, Łukasz Kondraciuk, Andrew Kondrich, Aris Konstantinidis, Kyle Koscic, Gretchen Krueger, Vishal Kuo, Michael Lampe, Ikai Lan, Teddy Lee, Jan Leike, Jade Leung, Daniel Levy, Chak Ming Li, Rachel Lim, Molly Lin, Stephanie Lin, Mateusz Litwin, Theresa Lopez, Ryan Lowe, Patricia Lue, Anna Makanju, Kim Malfacini, Sam Manning, Todor Markov, Yaniv Markovski, Bianca Martin, Katie Mayer, Andrew Mayne, Bob McGrew, Scott Mayer McKinney, Christine McLeavey, Paul McMillan, Jake McNeil, David Medina, Aalok Mehta, Jacob Menick, Luke Metz, Andrey Mishchenko, Pamela Mishkin, Vinnie Monaco, Evan Morikawa, Daniel Mossing, Tong Mu, Mira Murati, Oleg Murk, David Mély, Ashvin Nair, Rei- ichiro Nakano, Rajeev Nayak, Arvind Neelakantan, Richard Ngo, Hyeonwoo Noh, Long Ouyang, Cullen O’Keefe, Jakub Pachocki, Alex Paino, Joe Palermo, Ashley Pantuliano, Giambattista Parascandolo, Joel Parish, Emy Parparita, Alex Passos, Mikhail Pavlov, Andrew Peng, Adam Perelman, Filipe de Avila Belbute Peres, Michael Petrov, Henrique Ponde de Oliveira Pinto, Michael, Pokorny, Michelle Pokrass, Vitchyr H. Pong, Tolly Powell, Alethea Power, Boris Power, Elizabeth Proehl, Raul Puri, Alec Radford, Jack Rae, Aditya Ramesh, Cameron Raymond, Francis Real, Kendra Rimbach, Carl Ross, Bob Rotsted, Henri Roussez, Nick Ryder, Mario Saltarelli, Ted Sanders, Shibani Santurkar, Girish Sastry, Heather Schmidt, David Schnurr, John Schulman, Daniel Selsam, Kyla Sheppard, Toki Sherbakov, Jessica Shieh, Sarah Shoker, Pranav Shyam, Szymon Sidor, Eric Sigler, Maddie Simens, Jordan Sitkin, Katarina Slama, Ian Sohl, Benjamin Sokolowsky, Yang Song, Natalie Staudacher, Felipe Petroski Such, Natalie Summers, Ilya Sutskever, Jie Tang, Nikolas Tezak, Madeleine B. Thompson, Phil Tillet, Amin Tootoonchian, Elizabeth Tseng, Preston Tuggle, Nick Turley, Jerry Tworek, Juan Felipe Cerón Uribe, Andrea Valalone, Arun Vijayvergiya, Chelsea Voss, Carroll Wainwright, Justin Jay Wang, Alvin Wang, Ben Wang, Jonathan Ward, Jason Wei, CJ Weinmann, Akila Welihinda, Peter Welinder, Jiayi Weng, Lilian Weng, Matt Wiethoff, Dave Willner, Clemens Winter, Samuel Wolrich, Hannah Wong, Lauren Workman, Sherwin Wu, Jeff Wu, Michael Wu, Kai Xiao, Tao Xu, Sarah Yoo, Kevin Yu, Qiming Yuan, Wojciech Zaremba, Rowan Zellers, Chong Zhang, Marvin Zhang, Shengjia Zhao, Tianhao Zheng, Juntang Zhuang, William Zhuk, and Barret Zoph. Gpt-4 technical report, 2024. 3

[33] OpenAI OpenAI. Gpt-4 technical report. *arXiv preprint*, 2023. 3

[34] Gilhan Park, WonJun Moon, Subeen Lee, Tae-Young Kim, and Jae-Pil Heo. Mitigating background shift in class-incremental semantic segmentation. *ECCV*, abs/2407.11859, 2024. 2

[35] Sarah Pratt, Rosanne Liu, and Ali Farhadi. What does a platypus look like? generating customized prompts for zero-shot image classification. 2022. 3

[36] Yiqiao Qiu, Yixing Shen, Zhuohao Sun, Yanchong Zheng, Xiaobin Chang, Weishi Zheng, and Ruixuan Wang. Sats: Self-attention transfer for continual semantic segmentation. *Pattern Recognition*, 138:109383, 2023. 6

[37] Alec Radford, JongWook Kim, Chris Hallacy, A. Ramesh, Gabriel Goh, Sandhini Agarwal, Girish Sastry, Askell Amanda, Pamela Mishkin, Jack Clark, Gretchen Krueger, and Ilya Sutskever. Learning transferable visual models from natural language supervision. *Cornell University - arXiv, Cornell University - arXiv*, 2021. 2

[38] Sylvestre-Alvise Rebuffi, Alexander Kolesnikov, Georg Sperl, and Christoph H. Lampert. icarl: Incremental classifier and representation learning. In *2017 IEEE Conference on Computer Vision and Pattern Recognition (CVPR)*, 2017. 2

[39] Tal Ridnik, Emanuel Ben-Baruch, Nadav Zamir, Asaf Noy, Itamar Friedman, Matan Protter, and Lihi Zelnik-Manor. Asymmetric loss for multi-label classification. In *Proceed-*

ings of the IEEE/CVF international conference on computer vision, pages 82–91, 2021. 6, 3

[40] Chao Shang, Hongliang Li, Fanman Meng, Qingbo Wu, Heqian Qiu, and Lanxiao Wang. Incrementer: Transformer for class-incremental semantic segmentation with knowledge distillation focusing on old class. In *Proceedings of the IEEE/CVF Conference on Computer Vision and Pattern Recognition*, pages 7214–7224, 2023. 2

[41] Ying Sheng, Shiyi Cao, Dacheng Li, Coleman Hooper, Nicholas Lee, Shuo Yang, Christopher Chou, Banghua Zhu, Lianmin Zheng, Kurt Keutzer, et al. S-lora: Serving thousands of concurrent lora adapters. *arXiv preprint arXiv:2311.03285*, 2023. 6

[42] Guangchen Shi, Yirui Wu, Jun Liu, Shaohua Wan, Wenhui Wang, and Tong Lu. Incremental few-shot semantic segmentation via embedding adaptive-update and hyper-class representation. In *Proceedings of the 30th ACM International Conference on Multimedia*, 2022. 2

[43] Yuanzhi Su, Siyuan Chen, and Yuan-Gen Wang. Balanced residual distillation learning for 3d point cloud class-incremental semantic segmentation. *arXiv preprint arXiv:2408.01356*, 2024. 2

[44] Onur Tasar, Yuliya Tarabalka, and Pierre Alliez. Incremental learning for semantic segmentation of large-scale remote sensing data. *IEEE Journal of Selected Topics in Applied Earth Observations and Remote Sensing*, PP:1–14, 2019. 2

[45] Onur Tasar, Yuliya Tarabalka, and Pierre Alliez. Incremental learning for semantic segmentation of large-scale remote sensing data. *IEEE Journal of Selected Topics in Applied Earth Observations and Remote Sensing*, PP:1–14, 2019. 1

[46] Thanh-Dat Truong, Hoang-Quan Nguyen, Bhiksha Raj, and Khoa Luu. Fairness continual learning approach to semantic scene understanding in open-world environments. *Advances in Neural Information Processing Systems*, 36:65456–65467, 2023. 2

[47] Huyong Wang, Huisi Wu, and Jing Qin. Incremental nuclei segmentation from histopathological images via future-class awareness and compatibility-inspired distillation. In *2024 IEEE/CVF Conference on Computer Vision and Pattern Recognition (CVPR)*, pages 11408–11417, 2024. 1

[48] Huyong Wang, Huisi Wu, and Jing Qin. Incremental nuclei segmentation from histopathological images via future-class awareness and compatibility-inspired distillation. In *Proceedings of the IEEE/CVF Conference on Computer Vision and Pattern Recognition*, pages 11408–11417, 2024. 2

[49] Zifeng Wang, Zizhao Zhang, Chen-Yu Lee, Han Zhang, Ruoxi Sun, Xiaoqi Ren, Guolong Su, Vincent Perot, Jennifer Dy, and Tomas Pfister. Learning to prompt for continual learning. In *Proceedings of the IEEE/CVF conference on computer vision and pattern recognition*, pages 139–149, 2022. 2

[50] Jia-Wen Xiao, Chang-Bin Zhang, Jiekang Feng, Xialei Liu, Joost van de Weijer, and Ming-Ming Cheng. Endpoints weight fusion for class incremental semantic segmentation. In *Proceedings of the IEEE/CVF Conference on Computer Vision and Pattern Recognition*, pages 7204–7213, 2023. 2

[51] Zhengyuan Xie, Haiquan Lu, Jia-Wen Xiao, Enguang Wang, Le Zhang, and Xialei Liu. Early preparation pays off: New classifier pre-tuning for class incremental semantic segmentation. *ECCV*, abs/2407.14142, 2024. 6, 7

[52] Shipeng Yan, Jiangwei Xie, and Xuming He. Der: Dynamically expandable representation for class incremental learning. In *Proceedings of the IEEE/CVF conference on computer vision and pattern recognition*, pages 3014–3023, 2021. 2

[53] Xingyi Yang, Daquan Zhou, Songhua Liu, Jingwen Ye, and Xinchao Wang. Deep model reassembly. *Advances in neural information processing systems*, 35:25739–25753, 2022. 2

[54] Ze Yang, Ruibo Li, Evan Ling, Chi Zhang, Yiming Wang, Dezhao Huang, Keng Teck Ma, Minhoe Hur, and Guosheng Lin. Label-guided knowledge distillation for continual semantic segmentation on 2d images and 3d point clouds. In *Proceedings of the IEEE/CVF International Conference on Computer Vision*, pages 18601–18612, 2023. 2

[55] Jingwen Ye, Yifang Fu, Jie Song, Xingyi Yang, Songhua Liu, Xin Jin, Mingli Song, and Xinchao Wang. Learning with recoverable forgetting. In *European Conference on Computer Vision*, pages 87–103. Springer, 2022. 2

[56] Jeongbeen Yoon, Dahyun Kang, and Minsu Cho. Semi-supervised domain adaptation via sample-to-sample self-distillation. In *Proceedings of the IEEE/CVF Winter Conference on Applications of Computer Vision*, pages 1978–1987, 2022. 2

[57] Chaohui Yu, Qiang Zhou, Jingliang Li, Jianlong Yuan, Zhibin Wang, and Fan Wang. Foundation model drives weakly incremental learning for semantic segmentation. In *Proceedings of the IEEE/CVF Conference on Computer Vision and Pattern Recognition*, pages 23685–23694, 2023. 2

[58] Chaohui Yu, Qiang Zhou, Jingliang Li, Jianlong Yuan, Zhibin Wang, and Fan Wang. Foundation model drives weakly incremental learning for semantic segmentation, 2023. 2

[59] Lu Yu, Bartłomiej Twardowski, Xialei Liu, Luis Herranz, Kai Wang, Yongmei Cheng, Shangling Jui, and Joost van de Weijer. Semantic drift compensation for class-incremental learning. In *2020 IEEE/CVF Conference on Computer Vision and Pattern Recognition (CVPR)*, 2020. 2

[60] Xiao Yu, Yan Fang, Yao Zhao, and Yunchao Wei. Ipseg: Image posterior mitigates semantic drift in class-incremental segmentation. *arXiv preprint arXiv:2502.04870*, 2025. 2, 6, 7

[61] Zhidong Yu, Wei Yang, Xike Xie, and Zhenbo Shi. Tikp: Text-to-image knowledge preservation for continual semantic segmentation. In *Proceedings of the AAAI Conference on Artificial Intelligence*, pages 16596–16604, 2024. 2

[62] Zhidong Yu, Wei Yang, Xike Xie, and Zhenbo Shi. Tikp: Text-to-image knowledge preservation for continual semantic segmentation. In *Proceedings of the AAAI Conference on Artificial Intelligence*, pages 16596–16604, 2024. 7

[63] Bo Yuan and Danpei Zhao. A survey on continual semantic segmentation: Theory, challenge, method and application. *IEEE Transactions on Pattern Analysis and Machine Intelligence*, 2024. 1, 2

[64] Anqi Zhang and Guangyu Gao. Background adaptation with residual modeling for exemplar-free class-incremental semantic segmentation. *ECCV*, abs/2407.09838, 2024. 6, 7

[65] Wentao Zhang, Yujun Huang, Weizhuo Zhang, Tong Zhang, Qicheng Lao, Yue Yu, Wei-Shi Zheng, and Ruixuan Wang. Continual learning of image classes with language guidance from a vision-language model. *IEEE Transactions on Circuits and Systems for Video Technology*, 2024. 2

[66] Zekang Zhang, Guangyu Gao, Zhiyuan Fang, Jianbo Jiao, and Yunchao Wei. Mining unseen classes via regional objectness: A simple baseline for incremental segmentation. *Advances in neural information processing systems*, 35:24340–24353, 2022. 6

[67] Danpei Zhao, Bo Yuan, and Zhenwei Shi. Inherit with distillation and evolve with contrast: Exploring class incremental semantic segmentation without exemplar memory. *IEEE Transactions on Pattern Analysis and Machine Intelligence*, 45(10):11932–11947, 2023. 2

[68] Danpei Zhao, Bo Yuan, and Zhenwei Shi. Inherit with distillation and evolve with contrast: Exploring class incremental semantic segmentation without exemplar memory. *IEEE Transactions on Pattern Analysis and Machine Intelligence*, 45(10):11932–11947, 2023. 2

[69] Zhaocheng Zheng, Jingmin Wei, Xuefeng Hu, Haidong Zhu, and Ram Nevatia. Large language models are good prompt learners for low-shot image classification. *arXiv preprint arXiv:2312.04076*, 2023. 2

[70] Bolei Zhou, Hang Zhao, Xavier Puig, Sanja Fidler, Adela Barriuso, and Antonio Torralba. Scene Parsing Through ADE20K Dataset. In *CVPR*, 2017. 6, 3

[71] Lanyun Zhu, Tianrun Chen, Jianxiong Yin, Simon See, and Jun Liu. Continual semantic segmentation with automatic memory sample selection. In *Proceedings of the IEEE/CVF Conference on Computer Vision and Pattern Recognition*, pages 3082–3092, 2023. 1

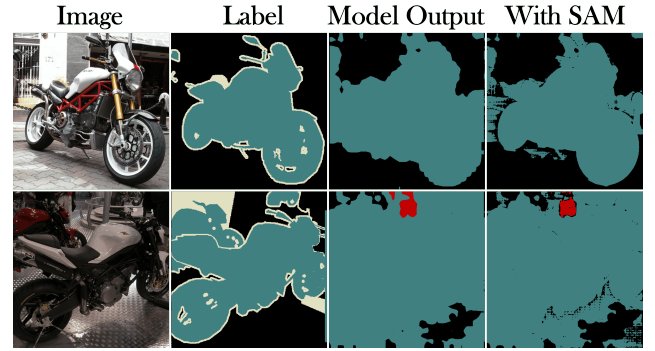
## A. Additional Experimental Results

### A.1. Additional Studies on Using SAM

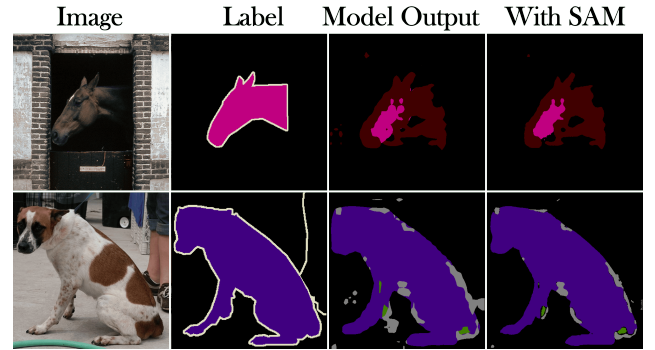
Although SAM is a powerful model, our method’s superior performance stems from how we integrate it rather than just its capabilities alone. We evaluated using fine-tuning SAM which was introduced in Sec. D to refine outputs from existing CSS methods. This limited gain reveals that merely applying SAM as a refinement module fails to harness its full potential, especially with CSS models whose performance degrades during incremental learning.

As Fig. A1 shows, we identified two key challenges when using SAM as a plug-and-play solution for CSS tasks: **Blurred Edges.** Ambiguous boundaries in CSS predictions compromise SAM’s effectiveness, as it relies on clear textural patterns for object delineation. When faced with blurred edges from CSS outputs, its extraction mechanism fails, as shown in Fig. A1a.

**Semantic Shift.** SAM’s class-agnostic segmentation creates limitations in CSS contexts where semantic shifts occur. As illustrated in Fig. A1b, SAM cannot correct semantic inconsistencies without class-specific understanding.



(a) Output cannot be refined as expected due to blurred edges



(b) SAM fails to correct semantic shifts in the output

Figure A1. PLOP results on VOC with 10-1 task setting, showing limitations of SAM refinement due to semantic shifts.

To further validate our approach, we compared against a Grounding DINO with fine-tune SAM baseline, providing class information to Grounding DINO during inference. (detailed in Sec. A.2).

### A.2. Grounding DINO with SAM

In this section, we design a new benchmark method that combines Grounding DINO with the SAM model. Specifically, we provide accurate category information for each image, using the output of Grounding DINO as a prompt for SAM segmentation.

On PASCAL VOC, the approach achieves 84% mIoU. This excellent performance is due to the relatively simple structure of the dataset, in that images typically contain only 1-2 target categories. Grounding DINO generates accurate bounding boxes, allowing SAM to segment precisely with minimal supervision. However, as shown by Fig. A2a line 5, SAM still struggles with suboptimal results due to the single-box prompt, as seen in Fig. A2a, which is more obvious in ADE dataset.

On the more complex ADE20K dataset, the benchmark’s performance drops to 57% mIoU. This is due to two main challenges: ADE20K’s multi-category nature complicates Grounding DINO’s ability to localize each class,

and SAM’s reliance on bounding boxes leads to hallucinations—incorrect segmentation. These issues highlight the difficulties and limitations of applying simple connection with SAM and Grounding DINO to complex segmentation tasks.

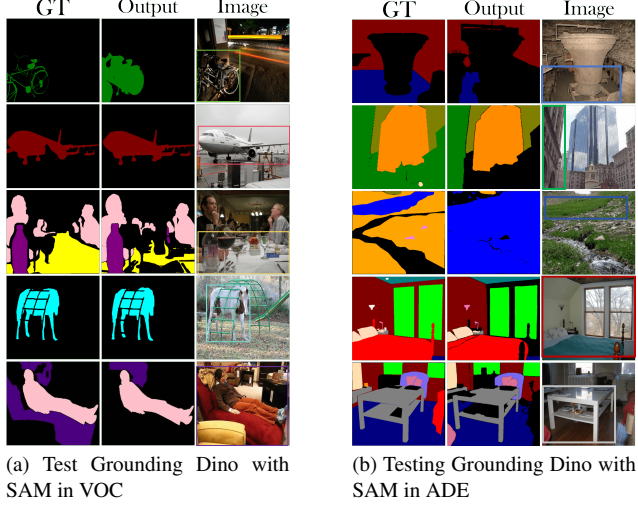


Figure A2. the stars with red outline are background points, the stars with green outline are foreground points

### A.3. Parameters Analysis

We calculate the parameter size of our method in Tab. A1. The table presents the parameter statistics for a single class pGen across different datasets. For the VOC dataset, each class-specific pGen accepts an input length of 512 and contains approximately 2.1 million parameters, requiring only 8MB of storage space when using float32 precision. For the ADE dataset, the input length increases to 1024, resulting in about 2.6 million parameters and 10MB of storage.

Datasets	Input length	Parameters	Size (MB)
VOC	512	2,097,152	8
ADE	1024	2,621,440	10

Table A1. pGen parameters for different datasets. The parameter size is calculated based on float32 (4 bytes per parameter).

### A.4. Visualization Analysis

pGen shared and class specific pGen, visualization in Fig. A3.

## B. Implementation Details

### B.1. Description of Classes

The following prompts were employed to generate concise, adjective-based descriptive phrases for each class. Our ap-

### Ground Truth      Prediction



Figure A3. Visualization in ADE with class-shared pGen. Left: Semantic shift phenomenon observed. Right: Generation of imprecise positional embeddings leading to poor segmentation.

proach leverages phrase-based descriptions rather than full sentences. This strategy is novel in that it constructs rich adjective+{class name} combinations to capture the essential visual features of each class. Such phrases have several CLASSEs over full sentences:

- They reduce computational load by saving tokens.
- They eliminate unnecessary grammatical words, thus focusing on key visual semantics.
- They provide a more flexible and enriched representation in the visual-language space. For example, while the token “dog” may cluster only with generic animal features, a phrase like “red dog” can better capture subtle distinctions, facilitating improved matching with diverse image scenarios.
- They enhance the meaningfulness of self-attention mechanisms by avoiding extraneous words (e.g., “there is a”) that do little to describe the class.

The following prompts were used:

1. “Generate a concise descriptive phrase for a(n) {CLASS}.”
2. “Provide a short adjective-based description for a(n) {CLASS}.”
3. “What is a brief phrase that captures the visual essence of a(n) {CLASS}?”
4. “Compose a succinct phrase highlighting the key characteristics of a(n) {CLASS}.”
5. “Summarize the appearance of a(n) {CLASS} using a short descriptive phrase.”
6. “Formulate an adjective+{class name} combination that best describes a(n) {CLASS}.”
7. “Identify a brief phrase that encapsulates the defining features of a(n) {CLASS}.”
8. “Express the distinctive visual traits of a(n) {CLASS} in a concise phrase.”

9. “What is the most representative adjective phrase for a(n) {CLASS}?”
10. “Create a short descriptive combination that emphasizes the visual attributes of a(n) {CLASS}.”
11. “For classes with synonymous forms (e.g., ‘man’, ‘woman’, ‘girl’ for person), generate a concise descriptive phrase considering these variations.”
12. “Taking into account synonymous terms for {CLASS}, produce a succinct descriptive phrase capturing the core visual features.”

In our experiments, we employ GPT-4 [32] and DeepSeek-V3 [12] to generate these phrases. An automated script is then used to filter and clean the outputs, ensuring the generated descriptions are both concise and semantically rich.

## B.2. Training Details

In training, we initialized our model with parameters from the Grounding DINO framework. Specifically, we leveraged the pre-trained image encoder, text encoder, and cross-attention component, with the latter referred to as the “Feature Enhancer” in the Grounding DINO paper. During the training process, we employed a task-specific LoRA strategy to fine-tune the cross-attention module while keeping both the image and text encoders frozen, which allows us to preserve the generalized feature extraction capabilities of the encoders while adapting the cross-modal interaction mechanism to our specific task requirements. We use CE loss function and Dice loss functions: Eq. (A.1)

During training, we adopted a multi-task learning strategy to optimize various model components. The primary loss function  $\mathcal{L}$  consists of a linear combination of cross-entropy (CE) and DICE losses, which jointly updates the parameters of the Class-specific pGen, task-specific LoRA adapters in cross-modal attention modules and the image encoder.

This primary loss Eq. (A.1) design effectively guides the model to generate accurate segmentation masks aligned with ground truth labels.

$$\begin{aligned} \mathcal{L} &= \mathcal{L}_{\text{Dice}} + \mathcal{L}_{\text{CE}} \\ &= 1 - \frac{2 \sum_{i=1}^N p_i g_i}{\sum_{i=1}^N (p_i^2 + g_i^2)} - \frac{1}{N} \sum_{i=1}^N \sum_{c=1}^C y_{ic} \log(p_{ic}). \end{aligned} \quad (\text{A.1})$$

Here,  $p_i$  denotes the predicted probability at the  $i$ -th pixel,  $g_i$  is the corresponding ground truth,  $y_{ic}$  is the one-hot encoded label for the  $i$ -th pixel for class  $c$ ,  $p_{ic}$  represents the predicted probability that the  $i$ -th pixel belongs to class  $c$ ,  $N$  is the total number of pixels, and  $C$  is the number of classes.

To derive classification results from the Similarity Matrix, we compute the average activation value across all im-

age tokens for each text embedding. Specifically, the classifier output vector  $\mathbf{r}$  is calculated as:

$$\mathbf{r}[j] = \frac{\sum_{i=1}^H \mathbf{S}'_i[i, j] \cdot \mathbb{1}(\mathbf{S}'_i[i, j] > 0)}{\sum_{i=1}^H \mathbb{1}(\mathbf{S}'_i[i, j] > 0)} \quad j \in \{1, 2, \dots, c_t\} \quad (\text{A.2})$$

where  $\mathbb{1}(\cdot)$  is the indicator function that equals 1 when the condition is true and 0 otherwise.

Simultaneously, we introduced Asymmetric Loss [39] as an auxiliary loss function Eq. (A.3), specifically designed to optimize the prediction  $\mathbf{r}$  and image category classification results. This loss function is particularly suitable for handling class imbalance in multi-label classification problems, effectively adjusting the model’s sensitivity to different categories. This dual-loss mechanism ensures that the model maintains category detection accuracy while generating high-quality location-aware prompts.

$$ASL(p, y) = \begin{cases} (1-p)^{\gamma_+} \log(p) & \text{if } y = 1 \\ p^{\gamma_-} \log(1-p) & \text{if } y = 0 \end{cases} \quad (\text{A.3})$$

## C. Dataset

**Datasets.** Our method was evaluated on two semantic segmentation datasets PASCAL VOC2012 [14] and ADE20K [70]. PASCAL VOC 2012 serves as a relatively straightforward benchmark containing 20 object classes plus a background class, containing 10,582 samples for training and 1,449 for validation, while ADE20K presents a more challenging scenario which is a large-scale semantic segmentation dataset with 150 annotated classes and one background class, containing 20,210 and 2,000 samples for training and validation.

## D. Fine-tuning SAM

Due to the fact that different datasets have different styles and annotation standards, using a frozen mask decoder cannot satisfy the requirement for generating high IoU masks. To address this issue, we employ a vanilla fine-tuning method with learning rate decay.

We observe that SAM’s segmentation performance under zero-shot conditions is significantly affected by dataset annotation styles, showing suboptimal performance on complex datasets. Therefore, we aim to fine-tune SAM to adapt to new data annotation patterns and improve its segmentation results.

The medical image segmentation field has presented many excellent examples and insights for fine-tuning SAM, where they apply LoRA to the Image Encoder while fine-tuning the Mask Decoder to adapt to their datasets.

Through our research, we find that modifications to the Image Encoder in medical imaging, which yield remark-

able results, are primarily necessary due to SAM’s insufficient training on medical image acquisition. Since we are working in the CSS domain, which doesn’t face these medical imaging-specific challenges, we reasonably hypothesize that fine-tuning only the **Mask Decoder** should be sufficient for SAM to adapt to CSS dataset(VOC,ADE).

We modify the semantic segmentation datasets to make them compatible with SAM’s training framework. As shown in Fig. D4, we transform the original semantic segmentation labels into instance-level masks with corresponding prompts (e.g., point or box prompts), allowing SAM to utilize these datasets effectively during fine-tuning. We also create separated labels to maintain SAM’s ability.

### D.1. Origin Label

In the ADE and VOC datasets, although it only provides segmentation labels without box or points, we can generate corresponding box prompts and point prompts from these labels. Point prompts can be divided into two categories: positive points placed on a specific label, and negative points placed within the box prompt but not on the corresponding label which is shown in Fig. D4a

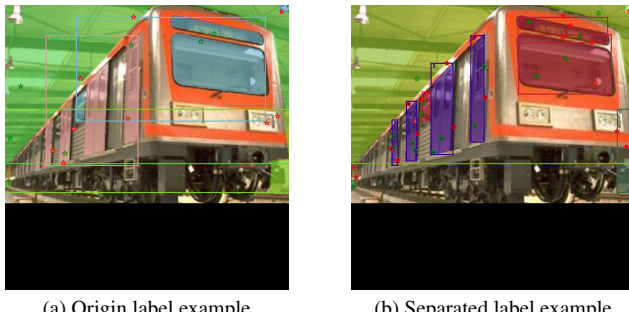


Figure D4. the stars with red outline are background points, the stars with green outline are foreground points

### D.2. Separated Label

With the aim to save grained ability for SAM, origin labels are separated based on whether they are in contact with other pixel with same label index, while excluding larger areas. We do the same prompt creating approach and example can be seen in Fig. D4b

### D.3. Fine-tuning Method in Mask Decoder

This fine-tuning strategy enables the mask decoder to better adapt to different dataset characteristics while maintaining model generalization ability, resulting in more accurate segmentation results.

#### Parameter Update Strategy:

- We fine-tune part of parameters of the mask decoder(don’t change the context embeddings)

- Use a small initial learning rate(1e-5) to maintain model stability
- Gradually decrease the learning rate during training to avoid performance degradation from excessive updates

### D.4. Loss

Our loss( Eq. (A.1)) is a linear combination of Dice loss and cross-entropy (CE) loss to supervise the mask prediction, balancing region overlap and pixel-level classification accuracy.